Contemporary Mathematics
Volume **549**, 2011

Finite Hamiltonian systems on phase space

Kurt Bernardo Wolf

Abstract. We construct and analyze a Hamiltonian system whose position coordinate takes values on the finite subset of contiguous integers $\mathcal{Z}_j := \{-j, -j+1, \ldots, j\}$, with the purpose of applying the resulting model to the parallel processing of finite, N-point signals by optical means, and for understanding models of finite quantum mechanics. Preserving the geometric and dynamic Hamilton equations of paraxial geometric optics, 'discrete quantization' leads us to the Lie algebra $\mathsf{so}(3)$, while the metaxial expansion by aberrations provides the rest of the N^2 unitary transformations that can be applied to any N-point signal. A compact phase space is the scenario for an $\mathsf{so}(3)$-covariant Wigner function to see such signals as nonlinear aberrations of the surface of a sphere.

1. Introduction

Over the last several years, our group in Cuernavaca has worked with geometric optics and —apparently disconnected— discrete models of quantum mechanics. Among the latter, finite N-point Hamiltonian systems are based on the well-known Lie algebra and group $\mathsf{so}(3)$, usually associated with rotations in space. Geometric optics and finite quantum mechanics are related through a 'quantization' process, distinct from the standard Schrödinger quantization of classical mechanics. Under this *finite* quantization, we associate to the observables of position, momentum, and energy, three $N \times N$ skew-hermitian matrices in a complex N-dimensional Hilbert space. These act on column vectors containing the data in the signal. We require that the geometry and dynamics of the classical system given by its Hamilton equations (written as Lie brackets) should be preserved under this finite-quantization process, and that in the limit $N \to \infty$, when the set of positions is contracted to the continuum, the original classical model should be recovered. The application of these endeavors is to provide models for finite signal analysis on phase space. In this essay we examine the finite analogue of the one-dimensional harmonic oscillator. The free particle and the repulsive oscillator, as well as a q-finite harmonic oscillator and two-dimensional models of pixellated screens have

1991 *Mathematics Subject Classification.* 20C35, 33C890, 37J35, 78A05, 81V99.
Key words and phrases. Lie group $\mathsf{SO}(3)$, Finite systems, Phase space.
I acknowledge the support of the *Óptica Matemática* projects (DGAPA-UNAM IN-105008 and SEP-CONACYT 79899). I is a pleasure to thank Guillermo Krötzsch (ICF-UNAM) for his indispensable help with the graphics.

been investigated; although referenced below, these topics will not be included here. We shall favor the narrative style of mathematical physics manuscripts; since the algebra $\mathsf{so}(3)$ is so well known, we need not develop a theorem-proof-corollary text, but only highlight the main results.

In Section 2 we detail the discrete quantization process for the three systems that classically have quadratic Hamiltonians, and lie under the ægis of the Lie algebras $\mathsf{so}(3)$, $\mathsf{iso}(2)$, and $\mathsf{so}(2,1)$, verifying that their contraction to the continuum limits returns the corresponding standard quantum and classical systems. We then review in Section 3 the ranges that the discrete position can have within each of these algebras, and their relation with the value of the Casimir invariant. The overlap between the position and energy bases provides the wavefunctions of the discrete system; in Section 4 we find the finite difference 'Schrödinger' equations that rule the three systems. Thereafter, from Section 5 we concentrate on the $\mathsf{so}(3)$ case of finite signals, where Kravchuk functions are the finite counterparts of the Hermite-Gauss eigenfunctions of the harmonic oscillator.

With these tools we examine in Section 6 the $\mathsf{SO}(3)$ 'linear' transformations such as the fractional Fourier-Kravchuk transform, and apply them in Section 7 to produce the sphere manifold —and phase space— of finite N-point coherent states. Now, whereas $\mathsf{SO}(3)$-linear transformations rotate this sphere rigidly, N-point signals can be acted upon by the group $\mathsf{U}(N)$ of $N \times N$ unitary matrices, as shown in Section 8; these will include all the *aberrations* of the signal as nonlinear area-preserving transformations of the surface of the sphere. The geometric optical classification and compounding of aberrations serves in Section 9 to define a new factored-product parametrization of $\mathsf{U}(N) \supset \mathsf{U}(2)$ into 'paraxial' and 'aberration' parameters. The identification of the sphere as the proper phase space for finite Hamiltonian systems is done in Section 10 by constructing a covariant Wigner function to represent graphically the action of aberrations on a discrete rectangle signal. The concluding Section 11 puts these developments in comparison with infinite discrete systems and other algebras used recently for signal analysis and the processing of pixellated images.

2. Discrete quantization

The strategy of *discrete quantization* from a classical system to a matrix realization of the corresponding discrete system is the following:

(i) We start with the well-recognized classical observables of position and momentum x, p with a Lie bracket that is their Poisson bracket (skew-symmetric, linearly distributive, with Leibniz rule),

$$\text{basic:} \qquad \{x,p\} = 1, \tag{2.1}$$

and $\{x,1\} = 0$, $\{p,1\} = 0$. Thus x, p, 1 are a basis for the Heisenberg-Weyl Lie algebra w [**1**].

(ii) With these quantities we build the quadratic Hamiltonians

$$h^{(\sigma)} := \tfrac{1}{2}(p^2 + \sigma x^2), \qquad \sigma = \begin{cases} +1, & \text{harmonic oscillator,} \\ 0, & \text{free particle,} \\ -1, & \text{repulsive oscillator.} \end{cases} \tag{2.2}$$

(iii) The two Hamilton equations,

$$\text{geometric:} \qquad \{h^{(\sigma)}, x\} = -p, \tag{2.3}$$

$$\text{dynamic:} \qquad \{h^{(\sigma)}, p\} = \sigma x, \tag{2.4}$$

together with (2.1), form semidirect products of w with rotations $\mathsf{so}(2)$ for $\sigma = +1$, translations $\mathsf{iso}(1)$ for $\sigma = 0$, and Lorentz boosts $\mathsf{so}(1,1)$ for $\sigma = -1$.

(iv) The crucial step now is to *deform* these three four-parameter Lie algebras to a direct sum of the central generator 1, with

$$\mathsf{so}(3) \qquad \text{for the harmonic oscillator } (\sigma = +1), \tag{2.5}$$

$$\mathsf{iso}(2) \qquad \text{for the free particle } (\sigma = 0), \text{ and} \tag{2.6}$$

$$\mathsf{so}(2,1) \qquad \text{for the repulsive oscillator } (\sigma = -1), \tag{2.7}$$

where position is chosen to be a *compact* generator in each algebra.

(v) Lastly, we choose a self-adjoint irreducible representation of each of these algebras, where the generators are represented as matrices and the Lie bracket is their commutator, to produce a discrete model for each of the three systems.

We postulate the following correspondence between classical observables and Lie algebra generators, setting up the notation

$$\text{position } x \quad \leftrightarrow \quad \mathcal{X} \equiv \mathcal{L}_0, \tag{2.8}$$

$$\text{momentum } p \quad \leftrightarrow \quad \mathcal{P} \equiv \mathcal{L}_1, \tag{2.9}$$

$$\text{(pseudo) energy } h \quad \leftrightarrow \quad \mathcal{K} \equiv \mathcal{L}_2, \tag{2.10}$$

and $1 \leftrightarrow \mathit{1}$ being the central generator of each algebra. We called $\mathcal{K}$ the *pseudo*-energy because its eigenvalues may (will) be displaced by some amount γ from the usual quantum-mechanical energies that are found from (2.2) through the Schrödinger quantization. The commutation relations to consider are thus

$$[\mathcal{K}, \mathcal{X}] = -\mathrm{i}\mathcal{P}, \qquad \text{(geometric Hamilton equation)}, \tag{2.11}$$

$$[\mathcal{K}, \mathcal{P}] = \mathrm{i}\sigma\mathcal{X}, \qquad \text{(dynamic Hamilton equation)}, \tag{2.12}$$

$$[\mathcal{X}, \mathcal{P}] = -\mathrm{i}\mathcal{K}, \qquad \text{(basic } \textit{nonstandard} \text{ commutator)}. \tag{2.13}$$

The quantization from Poisson brackets to commutators is through $\{u, v\} = w \leftrightarrow [U, V] = \mathrm{i}W$, so that with (2.8)–(2.10) the two Hamilton equations (2.3) and (2.4) translate to (2.11) and (2.12), consistently with the classical Hamiltonians (2.2) becoming the standard Schrödinger Hamiltonians. In the standard cyclic-index form, these Lie algebras are characterized by

$$[\mathcal{L}_0, \mathcal{L}_1] = -\mathrm{i}\mathcal{L}_2, \quad [\mathcal{L}_1, \mathcal{L}_2] = -\mathrm{i}\sigma\mathcal{L}_0, \quad [\mathcal{L}_2, \mathcal{L}_0] = -\mathrm{i}\mathcal{L}_1. \tag{2.14}$$

Finally, the invariant Casimir operator of these algebras is

$$\mathcal{C} := \sigma\mathcal{X}^2 + \mathcal{P}^2 + \mathcal{K}^2 = \sigma\mathcal{L}_0^2 + \mathcal{L}_1^2 + \mathcal{L}_2^2 = \gamma\mathit{1}, \tag{2.15}$$

where γ determines (not quite) uniquely an irreducible representation of the algebra, in each of the three cases. This γ will be used to relate the energy-numbers to the pseudo-energy eigenvalues, below.

We now show that under contraction $\gamma \to \infty$, we recover the Schrödinger operators of each system. Let

$$\mathcal{X}_\gamma := \gamma^{-1/4}\mathcal{X}, \quad \mathcal{P}_\gamma := \gamma^{-1/4}\mathcal{P}, \quad \mathcal{K}_\gamma := \mathcal{K} + \gamma^{1/2}\mathit{1}. \tag{2.16}$$

When $\gamma \to \infty$, the geometric and dynamic Hamilton equations in (2.11) and (2.12) between $\mathcal{X}_\gamma, \mathcal{P}_\gamma, \mathcal{K}_\gamma$ remain invariant, as they should. Meanwhile (2.13) becomes the Heisenberg commutator,

$$[\mathcal{X}_\gamma, \mathcal{P}_\gamma] = \frac{1}{\sqrt{\gamma}}[\mathcal{X}, \mathcal{P}] = -\frac{\mathrm{i}}{\sqrt{\gamma}}(\mathcal{K}_\gamma - \sqrt{\gamma}\,1) \xrightarrow[\gamma\to\infty]{} \mathrm{i}1, \tag{2.17}$$

where the limit is weakly valid in the space of functions with bounded energy [*i.e.*, $(f, \mathcal{K}^2 f) < \infty$ with the inner product defined below in (3.1)]. Such proviso is also required when contracting finite to integral Fourier transforms (see *e.g.* [**4**, Sect. 3.4.5]). Next we write the Casimir operator (2.15), $\mathcal{C} = \gamma 1$, which is

$$\begin{aligned} \gamma 1 &= \sqrt{\gamma}\mathcal{P}_\gamma^2 + \sigma\sqrt{\gamma}\mathcal{X}_\gamma^2 + (\mathcal{K}_\gamma - \sqrt{\gamma}1)^2 \\ &= \sqrt{\gamma}(\mathcal{P}_\gamma^2 + \sigma\mathcal{X}_\gamma^2 - 2\mathcal{K}_\gamma) + \mathcal{K}_\gamma^2 + \gamma 1, \end{aligned} \tag{2.18}$$

$$\Longrightarrow \qquad \mathcal{K}_\gamma = \tfrac{1}{2}(\mathcal{P}_\gamma^2 + \sigma\mathcal{X}_\gamma^2) + \frac{1}{2\sqrt{\gamma}}\mathcal{K}_\gamma^2, \tag{2.19}$$

with the same condition of validity.

The relation between the energy eigenvalue η of $\mathcal{K}_\gamma$ in (2.19), and the pseudo-energy eigenvalue λ of $\mathcal{K}$ obtained with $\mathcal{K}_\gamma = \mathcal{K} + 1\sqrt{\gamma}$ can be assumed to hold for all γ's, not necessarily in contraction. Thus, for each of the three algebras (2.5)–(2.7), although the expression for γ is slightly different, the relation between energy and pseudo-energy can have the generic form

$$\eta \approx \lambda + \sqrt{\gamma} + \text{constant}. \tag{2.20}$$

3. Ranges for discrete positions

Discrete systems are characterized by difference equations, rather than the differential ones of continuous mechanics. These equations stem from the algebra when we ask for the discrete eigenfunctions of its generators, and thus determine that their spacing be unity. The discrete wavefunctions (that we may also call *signals*, or *states* of the system) are $f_m \equiv f(x_m)$, with the argument $x_m = m$ running over the integer spectrum of the position operator, $\Sigma(\mathcal{X})$. These states live in complex Hilbert spaces of square-summable sequences $\ell^2(\mathcal{Z})$, or $\ell^2(\mathcal{Z}_0^+)$, or $\mathcal{C}^N$ when the space is of finite dimension N. They are endowed with the usual inner product and norm,

$$(f, g) := \sum_{m\in\Sigma(\mathcal{X})} f_m^*\, g_m = (g, f)^*, \qquad |f| := \sqrt{(f, f)}. \tag{3.1}$$

In these spaces, the generators (2.8)–(2.10) and the Casimir operator (2.15) should be self-adjoint, and thus their spectra real. In particular, the compact position $\mathcal{X} = \mathcal{L}_0$, has a natural Kronecker basis of eigenvectors in these Hilbert spaces given by the simultaneous eigenvectors of position and of the Casimir operator,

$$\mathcal{L}_0\, f_m^\gamma = m\, f_m^\gamma, \quad m \in \mathcal{Z}, \qquad \mathcal{C}\, f_m^\gamma = \gamma\, f_m^\gamma. \tag{3.2}$$

We can picture them as finite or infinite column vectors of 0's with a single 1 at position m.

The algebraic relations leading to the difference 'Schrödinger' equations are known for the three algebras (2.5)–(2.7), but we shall rederive them succintly, One defines the raising and lowering operators

$$\mathcal{L}_\uparrow := \mathcal{L}_2 + \mathrm{i}\mathcal{L}_1, \qquad \mathcal{L}_\downarrow := \mathcal{L}_2 - \mathrm{i}\mathcal{L}_1, \tag{3.3}$$

which are adjoints of each other and whose commutators are, from (2.14),

$$[\mathcal{L}_0, \mathcal{L}_\updownarrow] = \pm\mathcal{L}_\updownarrow, \qquad [\mathcal{L}_\uparrow, \mathcal{L}_\downarrow] = 2\sigma\mathcal{L}_0. \tag{3.4}$$

The role of these operators is to shift the Kronecker wavefunctions up or down by one unit,

$$\mathcal{L}_{\uparrow\downarrow}\, f^\gamma_m = c^\gamma_{\uparrow\downarrow m}\, f^\gamma_{m\pm1}, \tag{3.5}$$

up to normalization constants $c^\gamma_{\uparrow\downarrow m}$ that must be found. This is done using the invariant Casimir operator (2.15),

$$\mathcal{C} := \mathcal{L}_1^2 + \mathcal{L}_2^2 + \sigma\mathcal{L}_0^2 = \mathcal{L}_{\uparrow\downarrow}\,\mathcal{L}_{\downarrow\uparrow} + \sigma\mathcal{L}_0(\mathcal{L}_0 \mp \mathit{1}), \tag{3.6}$$

which constrains the ranges of γ and m through a well-known line of reasoning [**5**]: since the absolute square of the coefficients in (3.5) must be positive,

$$\begin{aligned} 0 \le |c^\gamma_{\uparrow\downarrow m}|^2 (f^\gamma_{m\pm1}, f^\gamma_{m\pm1}) &= (\mathcal{L}_{\uparrow\downarrow} f^\gamma_m, \mathcal{L}_{\uparrow\downarrow} f^\gamma_m) \\ &= (f^\gamma_m, \mathcal{L}_{\downarrow\uparrow}\mathcal{L}_{\uparrow\downarrow} f^\gamma_m) \\ &= (f^\gamma_m, [\mathcal{C} - \sigma\mathcal{L}_0(\mathcal{L}_0 \pm \mathit{1})]\, f^\gamma_m) \\ &= [\gamma - \sigma m(m\pm1)]\,(f^\gamma_m, f^\gamma_m), \\ \Longrightarrow \quad |c^\gamma_{\uparrow\downarrow m}|^2 &= \gamma - \sigma m(m\pm1) \ge 0. \end{aligned} \tag{3.7}$$

It follows that if some $c^\gamma_{\downarrow m_{\min}} = 0$, the equally-spaced spectrum of $\mathcal{X} = \mathcal{L}_0$ will be bounded from below by $m_{\min}$, while if some other $c^\gamma_{\uparrow m_{\max}} = 0$, its spectrum will be bounded from above by $m_{\max}$. Note carefully that (3.7) determines the coefficients $c^\gamma_{\uparrow\downarrow m}$ only up to a phase, which we are completely free to choose, although standard conventions exist; *e.g.*, see Ref. [**5**, p. 35].

From (3.7) and the condition that the m's of position be integer, one can identify its ranges and those of the representation index γ for the three algebras (2.5)–(2.7) distinguished by their value of σ,

$$\begin{array}{ll} \mathsf{so}(3) & \gamma = j(j+1), \quad j \in \mathcal{Z}_0^+, \quad |m| \le j, \\ \sigma{=}1 & \text{representation of dimension } N = 2j+1; \end{array} \tag{3.8}$$

$$\begin{array}{ll} \mathsf{iso}(2) & \gamma = l^2, \quad l \in \mathcal{R}, \quad m \in \mathcal{Z}, \\ \sigma = 0 & \text{infinite-dimensional representation;} \end{array} \tag{3.9}$$

$$\begin{array}{ll} \mathsf{so}(2,1) & \gamma = k(1-k) < \tfrac{1}{4}, \quad k \in \mathcal{Z}^+, \quad m \in \pm\{k,\, k{+}1, \ldots\}, \\ \sigma = -1 & \text{complementary series } D^\pm_k, \end{array} \tag{3.10}$$

$$\begin{array}{ll} & \gamma = k(1-k) \ge \tfrac{1}{4}, \quad k = \tfrac{1}{2}{+}\mathrm{i}\kappa,\ \kappa \in \mathcal{R}, \quad m \in \mathcal{Z}, \\ & \text{principal series } C^0_\kappa. \end{array} \tag{3.11}$$

This is a simplified list, because $\mathsf{so}(2,1)$ representations have further structure in the exceptional interval $0 \le k \le 1$, and because the algebras $\mathsf{so}(3)$ and $\mathsf{so}(2,1)$ also generate the 2:1 covering groups $\mathsf{SU}(2)$ and $\mathsf{SU}(1,1)$ where m runs over half-integers, while $\mathsf{ISO}(2)$ and $\mathsf{SO}(2,1)$ also have infinite covers, where the m's are not integer but spaced by 1.

4. Difference and Schrödinger equations

Beside the Kronecker basis of definite position, there are the energy eigenbases of $\mathcal{K} \equiv \mathcal{L}_2$ in (2.10), —implicitly distinguished by $\sigma \in \{+1, 0, -1\}$ for the three systems,

$$\mathcal{K}\, h^\gamma_\lambda = \lambda\, h^\gamma_\lambda, \quad \lambda \in \mathcal{Z} \text{ or } \mathcal{R}, \qquad \mathcal{C}\, h^\gamma_\lambda = \gamma\, h^\gamma_\lambda, \tag{4.1}$$

plus the proviso that in (3.11) for $\mathsf{so}(2,1)$ there is an extra dichotomic index to distinguish between two degenerate λ's in that spectrum.

Now, the overlap between the eigenbases of position $\{f^\gamma_m\}$ in (3.2), and of the energy $\{h^\gamma_\lambda\}$ in (4.1), defines the discrete *eigenfunctions* of the corresponding system,

$$\Psi^\gamma_\lambda(m) := (f^\gamma_m,\, h^\gamma_\lambda). \tag{4.2}$$

These functions satisfy the recurrence relation obtained from (3.3) and (3.5):

$$\begin{aligned} \lambda\Psi^\gamma_\lambda(m) &= (f^\gamma_m,\, \mathcal{K}\, h^\gamma_\lambda) \\ &= \tfrac{1}{2}([\mathcal{L}_\uparrow + \mathcal{L}_\downarrow]\, f^\gamma_m, h^\gamma_\lambda) \\ &= \tfrac{1}{2} c^{\gamma\ *}_{\uparrow\, m} \Psi^\gamma_\lambda(m{+}1) + \tfrac{1}{2} c^{\gamma\ *}_{\downarrow\, m} \Psi^\gamma_\lambda(m{-}1). \end{aligned} \tag{4.3}$$

To turn this recurrence into a difference equation, we must decide on the phases of the coefficients $c^\gamma_{\updownarrow,m}$ to obtain the correct contraction limit below,

$$c^{\gamma\ *}_{\uparrow\, m} = \varphi_\uparrow \sqrt{\gamma - \sigma m(m{+}1)}, \quad c^{\gamma\ *}_{\downarrow\, m} = \varphi_\downarrow \sqrt{\gamma - \sigma m(m{-}1)}, \tag{4.4}$$

with $|\varphi_\uparrow| = 1 = |\varphi_\downarrow|$. Then (3.7) leads to a three-term difference time-independent 'Schrödinger' equation in discrete position,

$$\begin{aligned} \varphi_\uparrow \sqrt{\gamma - \sigma m(m{+}1)}\, \Psi^\gamma_\lambda(m{+}1) + 2\lambda \Psi^\gamma_\lambda(m) \\ + \varphi_\downarrow \sqrt{\gamma - \sigma m(m{-}1)}\, \Psi^\gamma_\lambda(m{-}1) = 0. \end{aligned} \tag{4.5}$$

The contraction (2.16)–(2.20) of the difference equation (4.5) recovers the usual quantum Schrödinger equations for the three systems with $\varphi_\uparrow = 1 = \varphi_\downarrow$. Indeed, following the first of Eqs. (2.16), denote the eigenvalues of $\mathcal{X}$ by m, those of $\mathcal{X}_\gamma$ by $x := \gamma^{-1/4} m$, and re-define the function $\psi(x) = \psi(\gamma^{-1/4} m) := \Psi^\gamma_\lambda(m)$. Then, for γ sufficiently large and $\delta := \gamma^{-1/4}$ we can expand (4.5) to order δ^2 with up-to-second x-derivatives of $\psi(x)$,

$$\Psi^\gamma_\lambda(m \pm 1) = \psi(x \pm \delta) \;\approx\; \psi(x) \pm \delta\, \psi'(x) + \tfrac{1}{2}\delta^2\, \psi''(x), \tag{4.6}$$

$$\sqrt{\gamma - \sigma m(m{\pm}1)} \;\approx\; \sqrt{\gamma} - \tfrac{1}{2}\sigma x^2 \mp \delta\, \sigma x - \tfrac{1}{8}\delta^2\, x^4. \tag{4.7}$$

This yields, upon replacement into (4.5) and truncation to second order in δ,

$$\tfrac{1}{2}(-\psi''(x) + \sigma x^2\, \psi(x)) = (\lambda + \sqrt{\gamma})\, \psi(x) = \eta\, \psi(x) \tag{4.8}$$

plus terms of order δ^2, which vanish as $\gamma \to \infty$.

Starting from the next section our main interest will be on finite signals within $\mathsf{so}(3)$; thus we present only the following brief description of results in the other two cases: $\mathsf{iso}(2)$ and $\mathsf{so}(2,1)$.

The $\mathsf{iso}(2)$ free system was developed in Ref. [**6**]. The difference equation (4.5) simplifies with $\sqrt{\gamma} = l$ being the representation label; its solutions are trigonometric functions sin or cos $m\theta$ with $m \in \mathcal{Z}$, $\cos\theta = \lambda/l$, and energy $\eta = \lambda + l \in [0, 2l]$. Hence, this case reduces essentially to Fourier series, which transform unitarily between Fourier coefficients in $\ell^2(\mathcal{Z})$ and periodic functions in $\mathcal{L}^2(-\pi, \pi]$. Phase

space a cylinder; coherent and cat states —with their smiles— are shown graphically in [**6**]. The time evolution kernel between initial points m and final points m' is given by a Bessel function $\mathrm{i}^n J_{|m-m'|}(lt)$.

In Ref. [**8**] we used the complementary series of the algebra $\mathsf{so}(2,1)$ [**7**] to describe the radial part of a two-dimensional discrete system, following a polar pixellation of the plane. The radial coordinate $r_m \propto \sqrt{m}$, $m \in \mathcal{Z}_k^+$, $k \in \mathcal{Z}^+$, turns out to be the Bargmann index k which is related to the Casimir eigenvalue (3.2) by $\gamma = k(1-k)$. (In Bargmann's classification [**9**] the complementary series is called *discrete* series, D_k^+; but using this name could here cause confusion.) The discrete radial oscillator wavefunctions are written in terms of Meixner polynomials in $\ell^2(\mathcal{Z}_0^+)$; their contraction $k \to \infty$ limits to the well-known Laguerre-exponential functions.

Another $\mathsf{so}(2,1)$ discrete system we have studied is the discrete repulsive oscillator [**10**]. It is based on the principal series of representations of the algebra (in Bargmann's nomenclature, they are called the *continuous* representation series C_κ^0). The continuous counterpart of this system is the quantum repulsive oscillator, which is characterized by having a potential barrier $\sim\ -\frac{1}{2}x^2$. The Casimir eigenvalue (3.2) is in this case $\gamma = \frac{1}{4}+\kappa^2$ or, in terms of the Bargmann index, $k = \frac{1}{2}+\mathrm{i}\kappa$, $\kappa \in \mathcal{R}$. The energy spectrum is continuous, $\eta = \lambda + \kappa \in \mathcal{R}$, and double: there are left- and right-moving solutions, which are separated by a dichotomic index. The eigenfunctions of the system are given with Gauss hypergeometric functions (not polynomials), which provide a Dirac basis for $\ell^2(\mathcal{Z})$. An interesting feature is that the asymptotic chirp behavior of the quantum repulsive oscillator, $\sim \exp(\mathrm{i}\frac{1}{2}x^2)$, is replaced by an upper oscillation frequency with period 4. One can see the distinct behavior of the wavefunctions that pass over (for $\eta > 0$), or partially penetrate and partially reflect from the repulsive barrier (for $\eta < 0$). Computational issues with infinite Dirac-orthonormal vectors remain to be resolved satisfactorily.

5. The case of $\mathsf{so}(3)$: finite signals

Both $\mathsf{iso}(2)$ and $\mathsf{so}(2,1)$ are the Lie algebras of noncompact Lie groups; the only compact case is ruled by $\mathsf{so}(3)$; the discrete harmonic oscillator is thus the only choice for the analysis of complex N-point finite signals $\mathbf{f} \in \mathcal{C}^N$. For dimension $N = 2j+1$, the $\mathsf{SO}(3)$ transformations will belong to the representation of 'spin' $j \in \mathcal{Z}_0^+$, whose Casimir eigenvalue is $\gamma = j(j+1)$, and there will be N integer pseudo-energies $-j \le \lambda \le j$. The difference equation (4.5) with $|\varphi_\uparrow| = 1 = |\varphi_\downarrow|$ becomes the standard difference $\mathsf{so}(3)$ relation [**5**, Eq. (3.84)],[1]

$$\begin{aligned}\sqrt{(j-m)(j+m+1)}\,\Psi_\lambda^{j(j+1)}(m+1) + 2\lambda\Psi_\lambda^{j(j+1)}(m) \\ + \sqrt{(j+m)(j-m+1)}\,\Psi_\lambda^{j(j+1)}(m-1) = 0,\end{aligned} \tag{5.1}$$

[1] Our $\mathcal{L}$'s differ by a sign from the standard Biedenharn-Louck $\mathsf{so}(3)$ commutators [**5**], written as $J \times J = \mathrm{i}J$.

whose normalized solutions are the Wigner *little-d* functions (5.7),

$$\Psi^j_n(m) = d^j_{\lambda,m}(\tfrac{1}{2}\pi) \qquad n := \lambda + j \in [0, 2j] \tag{5.2}$$

$$= \frac{(-1)^n\,(2j)!\,{}_2F_1(-n,\,-2j{-}m;\,-2j;\,2)}{2^j\sqrt{n!\,(2j{-}n)!\,(j{+}m)!\,(j{-}m)!}} \tag{5.3}$$

$$= \frac{(-1)^n}{2^j}\sqrt{\binom{2j}{n}\binom{2j}{j+m}}\;K_n(j{+}m;\,\tfrac{1}{2},\,2j), \tag{5.4}$$

where the integer n is the energy *number* and $\eta = n + \frac{1}{2} \approx \lambda + \sqrt{\gamma}$ is the energy (2.20) of the finite oscillator model [**11**], the values of the position coordinate are $-j \le m \le j$, and

$$K_n(j{+}m;\tfrac{1}{2},2j) = {}_2F_1(-n,\;-2j{+}m;-2j;2) = K_{j+m}(n;\tfrac{1}{2},2j) \tag{5.5}$$

is a symmetric Kravchuk polynomial [**12, 13**] of degree n in the position coordinate m. These N wavefunctions are real, orthogonal and complete in $\mathcal{C}^N$, and normalized to satisfy

$$(\Psi^j_n, \Psi^j_{n'})_{\mathrm{so}(3)} := \sum_{m=-j}^{j} \Psi^j_n(m)^*\,\Psi^j_{n'}(m) = \delta_{n,n'}. \tag{5.6}$$

For future reference we write explicitly the Wigner *little-d* functions [**5**, Eq. (3.72)] for the generic rotation angle β,

$$\begin{aligned} d^j_{m,m'}(\beta) &= \sqrt{(j+m)!\,(j-m)!\,(j+m')!\,(j-m')!}\,(\sin\tfrac{1}{2}\beta)^{2j} \\ &\quad\times\sum_s \frac{(-1)^{j-m'-s}(\cot\tfrac{1}{2}\beta)^{m+m'+2s}}{s!\,(j-m-s)!\,(j-m'-s)!\,(m+m'+s)!}. \end{aligned} \tag{5.7}$$

A picture is worth a thousand words: the finite oscillator wavefunctions (5.2)–(5.4) are shown in Figure 1. Foremost we note that the lowest energy states resemble the Hermite-Gauss functions of the continuous quantum oscillator, while the highest-energy states reproduce the lowest, but for a change of sign between every two neighboring points, $\Psi^j_{2j-n}(m) = (-1)^{n+m}\Psi^j_n(m)$ due to identities between little-d functions in (5.2). The expression (5.4) for $\Psi^j_n(m)$ contains the square root of a binomial distribution in the position m; when we contract $j \to \infty$ through $x = m/\sqrt{j}$ [**14**], this factor becomes the standard Gaussian bell $\sim \exp(-\frac{1}{2}x^2)$. Under the same contraction, Kravchuk polynomials in m become Hermite polynomials in x. The ground state of the finite oscillator is

$$\Psi^j_0(m) = d^j_{-j,m}(\tfrac{1}{2}\pi) = \frac{1}{2^j}\sqrt{\frac{(2j)!}{(j{+}m)!\,(j{-}m)!}}, \tag{5.8}$$

and will serve below as the stationary coherent state. Out of translation in position and momentum we shall define below the manifold of coherent states of this model.

6. SO(3)-linear transformations of finite signals

To examine the dynamics we exponentiate the so(3) algebra of observables $\mathcal{X}$, $\mathcal{P}$, $\mathcal{K}$ to the Lie group SO(3) of all rigid rotations of a sphere. The 'z-' or 'time' evolution of discrete systems described by the Lie algebra so(3) in (2.11)–(2.13) is generated by $\mathcal{K}$ (plus $\sqrt{\gamma}1$, which generates only a phase), while translation in

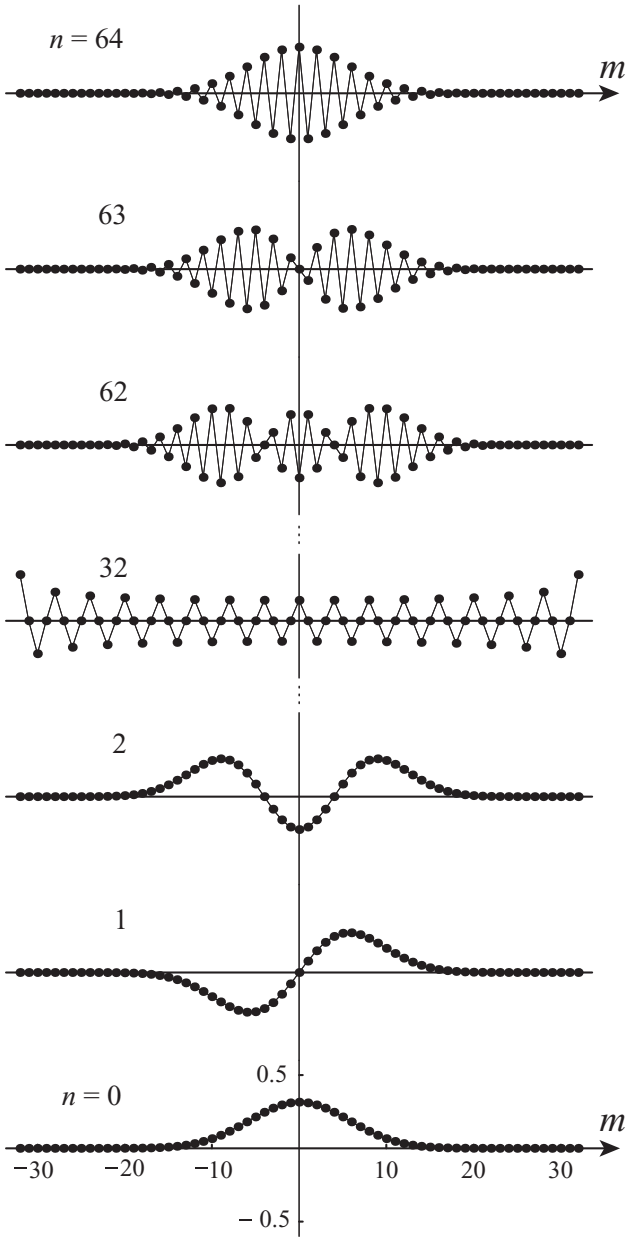

FIGURE 1. Finite oscillator wavefunctions $\Psi_n^j(m)$ in (5.3) for $N = 65$ points. From bottom to top, $n = 0, 1, 2, \ldots, 32, \ldots, 62, 63, 64 = 2j$. The ground state is $\Psi_0^j(m)$ in (5.8); the top state $\Psi_{2j}^j(m) = (-1)^m \Psi_0^j(m)$ is the highest-energy waveform that the system can carry.

position and momentum (x, p) are generated by $\mathcal{P}$ and $-\mathcal{X}$ respectively. When we

write the generic element of $\mathsf{so}(3)$ as

$$\mathcal{A}(x,p,z) = x\mathcal{X} + p\mathcal{P} + \kappa\mathcal{K}, \tag{6.1}$$

then its $\mathcal{K}$-evolution is

$$\exp(-\mathrm{i}\alpha\mathcal{K})\,\mathcal{A}(x,p,\kappa)\,\exp(+\mathrm{i}\alpha\mathcal{K}) = \mathcal{A}(x(\alpha),p(\alpha),\kappa(\alpha)), \tag{6.2}$$

producing a right-hand rotation of the sphere $x^2+p^2+\kappa^2 = r^2$ constant around the 'vertical' κ-axis by α,

$$\begin{pmatrix} x(\alpha) \\ p(\alpha) \\ \kappa(\alpha) \end{pmatrix} = \begin{pmatrix} \cos\alpha & \sin\alpha & 0 \\ -\sin\alpha & \cos\alpha & 0 \\ 0 & 0 & 1 \end{pmatrix} \begin{pmatrix} x \\ p \\ \kappa \end{pmatrix}. \tag{6.3}$$

Similarly, 'translations' along the compact x and p coordinates are here rotations around the $-p$ and x axes, and are generated by $-\mathcal{P}$ and $\mathcal{X}$. Thus, generic N-point signals are transformed by the unitary irreducible representation matrices of the $\mathsf{SO}(3)$ group, known as Wigner *Big-D* matrices $D^j_{m,m'}(\mathbf{R})$, where $\mathbf{R}$ is a 3×3 orthogonal matrix of unit determinant, such as (6.3), which can be conveniently parametrized with the Euler angles (α,β,γ) around the κ-p-κ axes, or with the polar parameters $(\rho,\,\hat{n}(\theta,\phi))$ of rotation by the angle ρ around the axis $\hat{n}(\theta,\phi)$ on the unit sphere.

The κ-evolution generated by $\mathcal{F}(\alpha) := e^{-\mathrm{i}\alpha j}\exp(-\mathrm{i}\alpha\mathcal{K})$ on the space of N-point signals ($N=2j+1$), multiplies the discrete oscillator wavefunctions (5.2) by phases $e^{-\mathrm{i}\alpha(j+\lambda)} = e^{-\mathrm{i}\alpha n}$. This is the $N\times N$ *fractional Fourier-Kravchuk* transform [**11**]. Due to (5.6), its matrix elements $\mathbf{F}^j(\alpha) = \|F^j_{m,m'}(\alpha)\|$ are given by the bilinear generating function,

$$F^j_{m,m'}(\alpha) := \sum_{n=0}^{2j} \Psi^j_n(m)\,\exp(-\mathrm{i}\alpha n)\,\Psi^j_n(m')^*. \tag{6.4}$$

The matrices $\mathbf{F}^j(\frac{1}{2}\pi)$ are $N\times N$ unitary fourth roots of unity. This was called *Fourier-Kravchuk* transform [**11**]; although this is *not the* discrete Fourier transform (DFT) matrix $\|e^{-2\pi\mathrm{i}mm'/N}/\sqrt{N}\|$, it is 'close': when $N\to\infty$, (6.4) becomes the Namias expression for the canonical fractional Fourier integral kernel [**15**]. The fractional Fourier-Kravchuk transform of the number eigenstate $\Psi^j_n(m)$ is thus $\exp(-\mathrm{i}\alpha n)\,\Psi^j_n(m)$, and the absolute values $|\Psi^j_n(m)|$ are *invariant* under the finite oscillator Hamiltonian evolution.

7. Finite coherent states

Waveforms that are *covariant* with the classical oscillator motion must have a parameter that evolves with a factor $\sim\exp(\pm\mathrm{i}\omega t)$. These are the coherent states, defined as the ground state $\Psi^j_0(m)$ in (5.8) and all its rotations by $\mathsf{SO}(3)$ group elements. In the Euler parametrization of rotations around successive axes, $\mathbf{R}(\alpha,\beta,\gamma) = \mathbf{R}_\kappa(\alpha)\,\mathbf{R}_p(\beta)\,\mathbf{R}_\kappa(\gamma)$, the rightmost factor multiplies $\Psi^j_0(m)$ only by a phase, which in this context is unimportant. The middle factor rotates the ground distribution around the p-axis, raising the bottom pole of the sphere ($x^2+p^2+\kappa^2 = r^2$ at $\kappa=-r$) up along the meridian containing the x-axis, and determining thus

the circle of discrete, finite coherent states for $-j \le m \le j$ and $-\pi < \beta \le \pi$,

$$\Upsilon^j(m;\beta) := \Big(\mathbf{R}_p(\beta)\,\Psi_0^j\Big)(m) \tag{7.1}$$

$$= \sum_{m'=-j}^{j} \Big(\exp(\mathrm{i}\beta\mathcal{P})\Big)_{m,m'}\, d^j_{-j,m'}(\tfrac{1}{2}\pi) \tag{7.2}$$

$$= d^j_{-j,m}(\tfrac{1}{2}\pi+\beta) \tag{7.3}$$

$$= \sum_{n=0}^{2j}(-1)^n d^j_{j,j-n}(\beta)\,\Psi^j_n(m). \tag{7.4}$$

In (7.2) the coherent state is recognized as a Wigner *little-d* function of angle $\frac{1}{2}\pi+\beta$. If we picture the ground state $\Upsilon^j(m;0)$ as a bell distribution centered at the bottom pole of the sphere, $\Upsilon^j(\cdot;\beta)$ can be pictured as this distribution centered at the colatitude $\pi-\beta$ in the direction of the x-axis. The form (7.4) expresses the coherent states as finite generating functions of $\Psi^j_n(m)$, summing over $n \in [0,2j]$, with coefficients that are obtained from (5.7),

$$(-1)^n d^j_{j,j-n}(\beta) = (\cos\tfrac{1}{2}\beta)^{2j}\sqrt{\binom{2j}{n}}\,(\tan\tfrac{1}{2}\beta)^n. \tag{7.5}$$

This account of coherent states should be compared with that in continuous quantum mechanics, where a generating function similar to (7.4) is formed with coefficients $c^n/\sqrt{n!}$ over $n \in \mathcal{Z}_0^+$. In the finite case we can identify the power-n coefficient to be $c \sim \tan\frac{1}{2}\beta$.

Lastly, the Euler rotation $\mathbf{R}_\kappa(\alpha)$ multiplies each n-summand in (7.4) by $\exp(-\mathrm{i}\alpha n)$; incorporating these phases into the coefficients (7.5) results in a factor $(e^{-\mathrm{i}\alpha}\sin\frac{1}{2}\beta)^n$. Based on this we can identify the parameter undergoing harmonic motion under the action of the finite oscillator Hamiltonian $\mathcal{K}$ as the coefficients $c(\alpha,\beta) := e^{-\mathrm{i}\alpha}\tan\frac{1}{2}\beta$. The finite coherent states (7.1)–(7.4) thus exhibit the harmonic motion resulting from the multiplication of $c(\alpha,\beta)$ by the phase $\exp(\mathrm{i}\tau)$. This is shown in Figures 2.

We can also speak of 'J_x-ground' and 'J_x-top states as the column N-vectors $(0,\ldots,0,1)^T$ and $(1,0,\ldots,0)^T$, which are particular cases of coherent states, namely: $\Upsilon^j(m;\pm\frac{1}{2}\pi) = d^j_{-j,m}(\pm\pi) = \delta_{m,j}$, the latter is shown at the top right of Fig. 2 that we picture on the sphere as a vector pointing along the $-x$-axis; its momentum and energy distributions now have the form (5.8) save for phases. Similarly, the 'J_p'-extremal momentum states will occur for $\beta = \frac{1}{2}\pi$ and $\alpha = \pm\frac{1}{2}\pi$, and their position and energy distributions will have the form (5.8).

8. Linear transformations and aberrations

Position, momentum and (pseudo)-energy are now represented by $N\times N$ matrices belonging to the representation j of $\mathsf{so}(3)$, $\mathbf{X} = \|X_{m,m'}\|$, $\mathbf{P} = \|P_{m,m'}\|$, and also $\mathbf{K} = \|K_{m,m'}\|$, with elements obtained from (3.2) and (3.5),

$$X_{m,m'} = m\,\delta_{m,m'}, \qquad m,\, m' \in \{-j,\, -j{+}1,\, \ldots,\, j\}, \tag{8.1}$$

$$P_{m,m'} = -\mathrm{i}\tfrac{1}{2}\sqrt{(j-m)(j+m+1)}\,\delta_{m+1,\,m'} + \mathrm{i}\tfrac{1}{2}\sqrt{(j+m)(j-m+1)}\,\delta_{m-1,\,m'}, \tag{8.2}$$

$$K_{m,m'} = \tfrac{1}{2}\sqrt{(j-m)(j+m+1)}\,\delta_{m+1,\,m'} + \tfrac{1}{2}\sqrt{(j+m)(j-m+1)}\,\delta_{m-1,\,m'}. \tag{8.3}$$

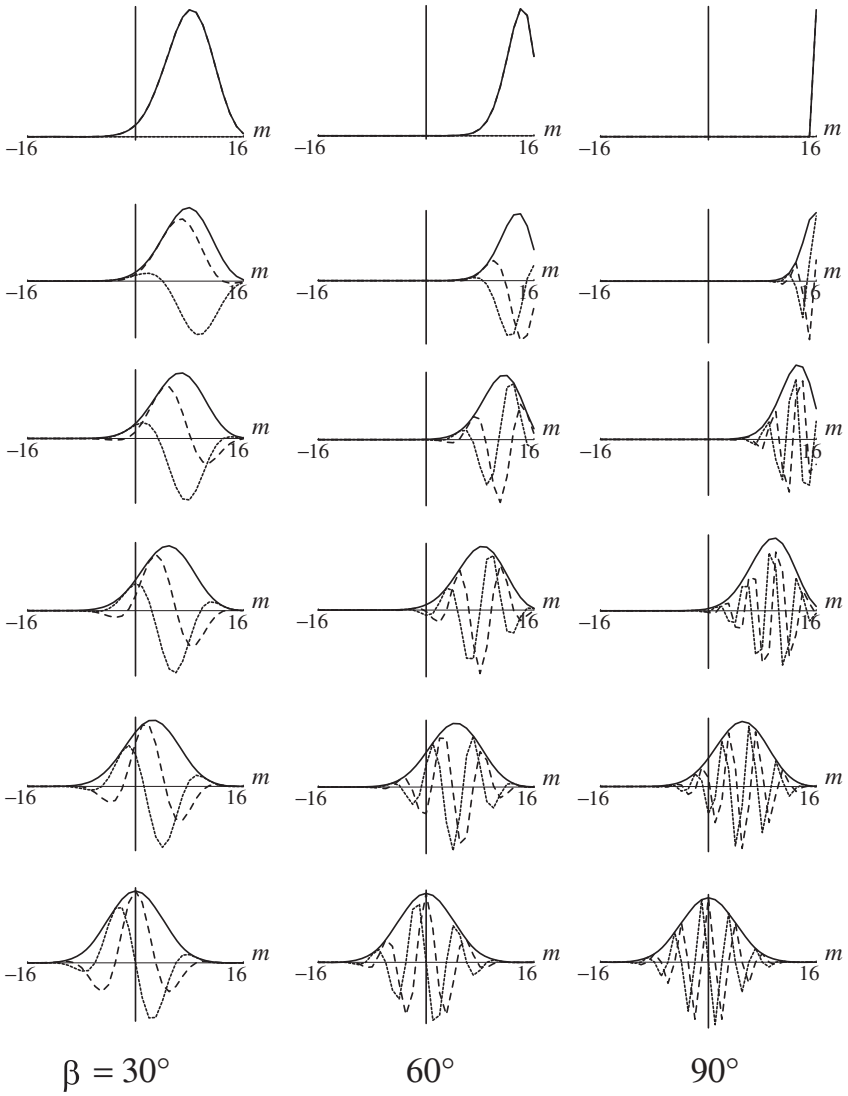

FIGURE 2. Quarter-cycle motion (top to bottom) of the coherent states $\Upsilon^j(m;\beta)$ in a finite oscillator of $N = 33$ points. Columns show these states for $\beta = 30° = \frac{1}{6}\pi$, $60° = \frac{1}{3}\pi$ and $90° = \frac{1}{2}\pi$. In the top right corner, the coherent state is an extreme-x Kronecker state.

These matrices are hermitian, traceless, satisfy the $\mathsf{so}(3)$ commutation relations, and their sum of squares (2.15) is $j(j+1)\mathbf{1}$. They multiply the column N-vectors $\mathbf{f}$ whose elements are the values of the signal. The position operator $\mathcal{X}$ is represented by the diagonal matrix $\mathbf{X}$ in (8.1); the momentum matrix $\mathbf{P}$ in (8.2) has the action of $-\mathrm{i}$ times a weighted central difference. And the pseudo-energy matrix $\mathbf{K}$ in (8.3) is real and symmetric. If we interpret the latter as the Hamiltonian matrix of a linear mechanical lattice of $2j+1$ mass points joined by springs, its sub-diagonal

elements are the interaction forces between the mass number m and its two nearest neighbors $m\pm1$ [**4**, Part I], and have the form $\sqrt{(\gamma - m(m\pm1))}$. This is (minus) the discrete gradient of an 'equivalent potential' function on $m \in [-j, j]$, which indeed has the parabolic bowl-shape characteristic of oscillator-like discrete systems (*cf.* the Harper discrete potential $\sim 1-\cos 2\pi m/N$ [**18**]). Since the ground state has no zeros, the equivalent potential can also be defined from the finite oscillator ground state (5.8), as its normalized second-difference $\Delta\Psi^j_0(m)/\Psi^j_0(m)$ [**17**].

The exponentiation of the linear combinations (6.1) of the $N\times N$ matrices (8.1)–(8.3) and **1**, generates a unitary irreducible representation the group $\mathsf{SO}(3)\otimes\mathsf{SO}(2)$. In the *polar* coordinates $(\rho,\, \hat{n}(\theta,\phi);\, \tau)$ of this group, the matrices are

$$\mathbf{R}(\rho,\theta,\phi;\tau) = \exp -\mathrm{i}(u\mathbf{X} + v\mathbf{P} + w\mathbf{K})\, e^{-\mathrm{i}\tau}, \qquad \begin{cases} u &= \rho\sin\theta\sin\phi, \\ v &= \rho\sin\theta\cos\phi, \\ w &= \rho\cos\theta. \end{cases} \tag{8.4}$$

These are the Wigner *Big-D* matrices [**5**], written with polar rather than Euler parameters; they carry the *linear* action of the group $\mathsf{SO}(3)$ on the space of N-point signals [**11, 13, 19**].

In geometric optics, the paraxial regime comprises all linear transformations of phase space $(x,p)\in\mathcal{R}^2$. These are generated by the Poisson operators $\{A_2,\circ\}$ of quadratic functions $A_2(x,p)$ (that form the noncompact symplectic algebra $\mathsf{sp}(2,\mathcal{R})$). The *metaxial* regime lies beyond the paraxial r'egime: it is generated by polynomials $A_n(x,p)$ of homogeneous degree n in x and p, called *aberrations* of order $A^{\mathrm{c}} = n-1$, for $n\in\{2,3,\ldots\}$; the transformations are nonlinear in phase space $(x,p)\in\mathcal{R}$, shown as a tower in Figure 3 [**20**, Fig. 13.1]. For discrete N-point Hamiltonian systems we propose that these nonlinear transformations be built out of the universal enveloping algebra $\overline{\mathsf{so}}(3)$ that contains all sums, powers and products of the $\mathsf{so}(3)$ generators $\{\mathcal{X},\,\mathcal{P},\,\mathcal{K}\}$, with the commutator Lie bracket that obeys the Leibniz rule, and within the representation j of $\mathsf{so}(3)$ determined by the Casimir operator (2.15). We use the last condition to reduce the count of powers of $\mathcal{K}$ to 0 or 1 only. The correspondence between the classical variables and the non-commuting matrices of the discrete model will be made through their *Weyl* ordering [**1**]. Thus, for $k\in\{\frac12, 1, \ldots, \frac12(N-1)\}$ we define the matrices

$$\mathbf{A}^{k,\mu;0} := \{\mathbf{P}^{k+\mu}\mathbf{X}^{k-\mu}\}_{\mathrm{Weyl}}, \qquad \mu\in\{-k, -k+1, \ldots, k\}, \tag{8.5}$$

$$\mathbf{A}^{k,\mu;1} := \{\mathbf{P}^{k-\frac12+\mu}\mathbf{X}^{k-\frac12-\mu}\mathbf{K}\}_{\mathrm{Weyl}}, \quad \mu\in\{-k+\tfrac12, -k+\tfrac32, \ldots, k-\tfrac12\}. \tag{8.6}$$

The Weyl order of a monomial of matrix powers $\{\mathbf{X}^a\mathbf{Y}^b\mathbf{Z}^c\}_{\mathrm{Weyl}}$ sums all permutations of the $a+b+c$ individual matrices, and divides by $(a+b+c)!$. These matrices include the $\mathsf{so}(3)$ generators of linear transformations $\mathbf{A}^{1/2,-1/2,0} = \mathbf{X}$, $\mathbf{A}^{1/2,1/2,0} = \mathbf{P}$, $\mathbf{A}^{1/2,0,1} = \mathbf{K}$ and phases $\mathbf{A}^{0,0,0} = \mathbf{1}$; beyond, are the *aberrations* of orders $A := 2k$. The order is so defined because $[\mathbf{A}^{k,\mu;c}, \circ]$, acting on the $\mathsf{so}(3)$ generators returns polynomials of homogeneous degree $2k$ in these variables. There are N^2 independent hermitian matrices that generate of the $N\times N$ unitary Lie algebra $\mathsf{u}(N)$; hence in N-point Hamiltonian systems there are aberration orders $0 < A = 2k \le N-1 = 2j$ only. In the contraction limit $j\to\infty$ to geometric optics, the $k=0$ pyramid grows and we recover the infinite tower of aberrations in Fig. 3, while the $k=\frac12$ pyramid withers between functions of finite energy. The aberration orders, counted with Poisson brackets, are $A^{\mathrm{c}} = 2k-1$, $k\in\{2,3,\ldots\}$.

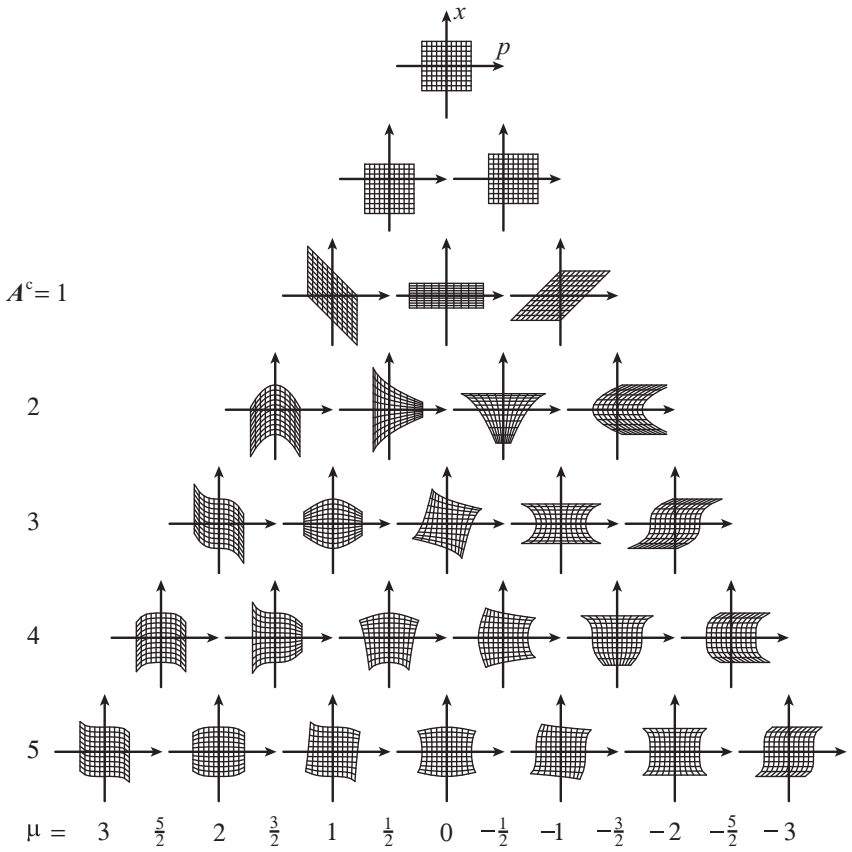

FIGURE 3. Tower of linear transformations and aberrations of classical phase space (x, p), generated by the exponentiated Poisson operators $\exp(\tau\{p^{k+\mu}x^{k-\mu}, \circ\})$. The rungs in the tower are classified by integer aberration order $A^c := 2k-1 \geq 0$ and *weight* μ, for $|\mu| \leq k$. The unit map is at the top; translations along x and p correspond to $A^c = 0$. The linear transformations are marked with $A^c = 1$; in paraxial geometric optics they are free propagation, (inverse) magnification, and a Fresnel lens. There follow the aberrations of orders $A^c = 2, 3, 4, 5\ldots$. In geometric optics, aligned systems produce only odd-order aberrations; for $A^c = 3$ these are named spherical aberration, coma, astigmatism/curvature of field, distorsion and pocus.

It is useful to present the concrete case of $N = 5$-point systems [**16**], where the Lie algebra $\mathsf{u}(5)$ has $5^2 = 25$ independent generators. Four of these are the generators of the $\mathsf{u}(2)$ subgroup of linear transformations, $A = 0, 1$; the rest can be organized into two pyramids for aberrations of orders $A = 2$, 3, and 4. We write their classical expressions (to be read with $x \to \mathbf{X}$, $p \to \mathbf{P}$, $\kappa \to \mathbf{K}$ and Weyl order)

as follows:

$$
\begin{array}{rccccccccc}
A^{k,\mu;0}(x,p)\text{:} & & & & & & & & & \\
A=0 & & & & & 1 & & & & k=0 \\
1 & & & & p & & x & & & \tfrac{1}{2} \\
2 & & & p^2 & & px & & x^2 & & 1 \\
3 & & p^3 & & p^2x & & px^2 & & x^3 & \tfrac{3}{2} \\
4 & p^4 & & p^3x & & p^2x^2 & & px^3 & & x^4 \quad 2 \\
\mu= & 2 & \tfrac{3}{2} & 1 & \tfrac{1}{2} & 0 & -\tfrac{1}{2} & -1 & -\tfrac{3}{2} & -2,
\end{array}
\tag{8.7}
$$

$$
\begin{array}{rccccccc}
A^{k,\mu;1}(x,p,\kappa)\text{:} & & & & & & & \\
A=1 & & & & \kappa & & & k=\tfrac{1}{2} \\
2 & & & \kappa p & & \kappa x & & 1 \\
3 & & \kappa p^2 & & \kappa px & & \kappa x^2 & \tfrac{3}{2} \\
4 & \kappa p^3 & & \kappa p^2 x & & \kappa p x^2 & & \kappa x^3 \quad 2 \\
\mu= & \tfrac{3}{2} & 1 & \tfrac{1}{2} & 0 & -\tfrac{1}{2} & -1 & -\tfrac{3}{2}.
\end{array}
\tag{8.8}
$$

There are 15 entries in the first pyramid (8.7), matching those shown in Figure 3, while the second pyramid (8.8) repeats the pattern with an extra κ and has 10 entries. These sum to the 25 generators of $\mathsf{u}(5)$. We shall call $(x,p,\kappa) \in \mathcal{R}^3$ the *meta*-phase space of $\mathsf{SO}(3)$ systems.

9. Paraxial / aberration parameters of $\mathsf{U}(N)$

The $N \times N$ hermitian matrices (8.5)–(8.6) are the N^2 generators of the N-dimensional self-adjoint representation of the Lie algebra $\mathsf{u}(N)$. They have been naturally separated into the four 'paraxial' generators of the subalgebra $\mathsf{u}(2) \subset \mathsf{u}(N)$, and the N^2-4 'aberration' generators of orders $A = 2k \in \{2, 3, 4, \ldots, N-1\}$. The commutatior of two aberration generators of orders A_1 and A_2 is of aberration order $A = A_1 + A_2 - 1$ modulo N. The generators of each aberration order form an ideal under commutation with the 'paraxial' $\mathsf{u}(2)$ generator matrices (8.1)–(8.3); indeed they form *multiplets* (bases for irreducible representation subspaces) of dimension $2A+1$ and transform between themselves as the solid spherical harmonics do under the rotation group [**5**]. Meanwhile, in the continuous model of geometric optics [**20**, Part 4], the aberrations form finite-dimensional multiplets under linear canonical transformations generated by the symplectic algebra $\mathsf{sp}(2,\mathcal{R})$. Thus, since the algebras are different, the commutators between the aberration generator matrices will differ from their geometric-optical counterparts. A pending task is to examine in detail this contraction of unitary to symplectic transformations when $N \to \infty$.

The hermitian matrices (8.5)–(8.6) of $\mathsf{u}(N)$ are exponentiated to unitary matrices in $\mathsf{U}(N)$, where one-parameter subgroups are

$$
\mathbf{U}^{k,m;c}(\alpha) := \exp(-\mathrm{i}\alpha\, \mathbf{A}^{k,m;c}) \in \mathsf{U}(N), \quad c \in \{0,1\}. \tag{9.1}
$$

The hermitian matrices $\mathbf{A}^{k,m;c}$ that are pure imaginary (containing only odd powers of $\mathbf{P}$) will generate real orthogonal matrices, forming the subgroup $\mathsf{SO}(N) \subset \mathsf{U}(N)$ that leaves real signals real. Thus we obtain a coordinate system for $\mathsf{U}(N)$ that separates into coordinates of $\mathsf{SO}(N)$ and coordinates of the space of cosets $\mathsf{U}(N)/\mathsf{SO}(N)$ (*cf.* [**21**]).

The 'paraxial' subgroup $\mathsf{U}(2) \subset \mathsf{U}(N)$ in (8.4) includes phases and linear transformations of the sphere, and serves as the 'core' for the *factored-product*

parametrization of $\mathsf{U}(N)$. (*Cf.* the factored-product parametrization that uses the symplectic group $\mathsf{Sp}(2,\mathcal{R})$ of paraxial geometric optics as the core for the in-principle infinite aberration expansion [**22, 23**]). The ideal of aberration order $a = 2k \geq 1$ has dimension $2a + 1 = 4k + 1$ and generates the manifold of unitary matrices

$$\mathbf{U}_k(A_k) := \exp\Big[-\mathrm{i}\Big(\sum_{\mu=-k}^{k=a/2} A^0_{k,\mu}\mathbf{A}^{k,\mu;0} + \sum_{\mu=-k}^{k=(a-1)/2} A^1_{k,\mu}\mathbf{A}^{k,\mu;1}\Big)\Big], \tag{9.2}$$

parametrized by the 'aberration' parameters $A_k := \{A^0_{k,\mu},\, A^1_{k,\mu}\}^k_{\mu=-k}$. In this notation and using (8.4), we write the factored-product parametrization of $\mathsf{U}(N)$ as

$$\mathbf{U}_N(A) = \mathbf{U}_{N-1}(A_{N-1}) \times \mathbf{U}_{N-2}(A_{N-2}) \times \times \mathbf{U}_2(A_2) \times \mathbf{R}(\rho,\theta,\phi;\tau), \tag{9.3}$$

where in the rightmost factor, the four coefficients $\{A^0_{1,1},\, A^0_{1,0},\, A^0_{1,-1};\, A^1_{0,0}\}$ are related to $\{\rho,\, \theta,\, \phi;\, \tau\}$ through (8.4).

The factored-product parametrization is distinct from that derived with the more usual chain of Gel'fand-Tsetlin coset decomposition $\mathsf{U}(k{+}1)/\mathsf{U}(k)$ [**24**], for $k = N{-}1, \ldots, 1$ [**25, 26**]. The factored-product parameters are taylored for the analysis of one-dimensional finite discrete signals under parallel processing by optical systems with aberrations; the prototipical model we have in mind is that of a linear array of N LEDs emitting a phase-controlled wavefield into a two-dimensional micro-optical device, whose output is sensed by a similar linear array of sensors. Since we have already characterized the optical elements of compound devices by their Hamilton-Lie aberration coefficients in [**20**, Sect. 14.5], their finite quantization should yield $N \times N$ matrices which will produce a corresponding output for every input signal. This can be applied to fractional Fourier transformer devices [**27**], three of whose configurations (with a lens, a mirror, or a waveguide) are given in Ref. [**20**, Chap. 15] with their aberration coefficients to order seven. How will they work and approximate the ordinary N-dimensional Fourier matrix of a microscopic array of LEDs? The matrices (9.3) have been manipulated numerically; we have not endeavored to find the generic relation between the set of aberration parameters A and the matrix elements of $\mathbf{U}(A)$; commercial symbolic manipulation programs are quite efficient in multiplying and exponentiating arbitrary matrices.

10. The phase space of finite systems

We favor graphical images to see the effect of aberrations on a phase space suited for finite signals, such as those in Figure 3 for continuous models. So once again we condense the construction of the $\mathsf{SO}(3)$-covariant Wigner function proposed in Ref. [**28, 29**] on the corresponding phase space. For classical phase space we know that when acted upon by the exponentiated Poisson operators $\exp\alpha\{A,\circ\}$ of the aberration monomials $A^{k,\mu}(x,p) := p^{k+\mu}x^{k-\mu}$, will deform along the lines of flow $A^{k,\mu}(x,p) = \text{constant}$. For finite systems a similar analysis can be made to find the lines of flow of rigid (linear) and nonrigid deformations (aberrations) of the surface of the sphere $x^2 + p^2 + \kappa^2 = r^2$. At the bottom pole $\kappa = -r$, this sphere is tangent to the classical phase space plane $(x,p) \in \mathcal{R}^2$, to which it limits when $j \to \infty$, as in (2.17)–(2.19), and the lines of flow on the sphere will osculate those on the plane. To exploit this correspondence we use the $\mathsf{so}(3)$ Berezin brackets between

commuting functions of x, p, κ, which are defined by

$$\{x,p\}_{\rm B}=\kappa,\quad \{p,\kappa\}_{\rm B}=x,\quad \{\kappa,x\}_{\rm B}=p. \tag{10.1}$$

They obey the same distributivity and Leibniz rule as the Poisson brackets, and generate a classical realization of the group $\mathsf{SO(3)}$ as (8.4), replacing $\mathbf{X}\leftrightarrow\{x,\circ\}_{\rm B}$, etc.

The invariant surfaces in $(x,p,\kappa)\in\mathcal{R}^3$ under any $\{A(x,p,\kappa),\circ\}_{\rm B}$ are the spheres $x^2+p^2+\kappa^2=r^2$ and $A(x,p,\kappa)=$ constant itself. Now consider corresponding (8.5)–(8.6) with the classical aberration generator monomials $A^{k,\mu;0}(x,p)$ and $A^{k,\mu;0}(x,p,\kappa)$, which are of the form $x^ap^b\kappa^c$, $a+b+c=A$, with $c=0$ or 1. The aberrations $(k,\mu;0)$ in the first pyramid (8.7) will thus leave invariant the cylinders $A^{k,\mu;0}(x,p)=$ constant, whose intersection with each invariant sphere determines the lines of flow in $\mathcal{R}^3$. As we see from (8.5), for $\mu=k$ these are planes normal to the p-axis, and for $\mu=-k$ normal to the x-axis; for all other $-k<\mu<k$, the functions $p^{k+\mu}x^{k-\mu}=$ constant cut the sphere into quadrants bounded by the planes $x=0=p$ —refer to Figure 4— with four disjoint sets of closed and nested curves which matchthe flows of Figure 3 at the bottom pole $\kappa=-r$. The aberration functions $(k,\mu;1)$ in the second pyramid (8.8), are linear in κ; hence $A^{k,\mu;1}(x,p,\kappa)=$ constant are *cones* which at every $\kappa=$ constant slice reproduce scaled the lines of flow of $A^{k-1/2,\mu-1/2;0}(x,p)$. At the bottom pole they *also* match the corresponding flows of Figure 3, but on the top pole $\kappa=r$ the flow is in the opposite direction. The aberrations in the second pyramid thus divide the flow on the sphere into octants for $-k<\mu<k$, since the previous quadrants are cut by the $\kappa=0$ invariant plane, and there are eight disjoint sets of closed and nested curves. Finally, the cases $\mu=\pm k$ exhibit four disjoint sets of curves. Thus the classical aberrations on the phase plane correspond 1:2 with the transformations of the surface of the sphere.

We now ask for covariance between the classical function on $\mathsf{SO(3)}$,

$$R_{\rm cl}(\rho,\theta,\phi;x,p,\kappa):=\exp[-{\rm i}(ux+vp+w\kappa)] \tag{10.2}$$

and the $N\times N$ matrix representation $\mathbf{R}(\rho,\theta,\phi)$ in (8.4). The polar $\mathsf{SO(3)}$ group parameters $g=\{u,\,v,\,w\}\equiv\{\rho,\theta,\phi\}$ given in that equation range over the manifold of this group (leaving aside the $\mathsf{U(1)}$ phase τ). Thus we build the matrix-valued bilinear generating function between the classical and the finite hamiltonian systems by integrating over the $\mathsf{SO(3)}$ group manifold,

$$\begin{aligned}\mathbf{W}(x,p,\kappa) &:= \int_{\rm SO(3)} {\rm d}^{\rm Haar}(\rho,\theta,\phi)\,\mathbf{R}(\rho,\theta,\phi)\,R_{\rm cl}(\rho,\theta,\phi;x,p,\kappa)^*\\ &= \int_{\rm SO(3)} {\rm d}^{\rm Haar}(\rho,\theta,\phi)\,\exp{\rm i}[u(x-\mathbf{X})+v(p-\mathbf{P})+w(\kappa-\mathbf{K})],\end{aligned} \tag{10.3}$$

with the normalized Haar measure for polar coordinates,

$${\rm d}^{\rm Haar}(\rho,\theta,\phi)=\tfrac{1}{|\mathsf{SO(3)}|}\,\tfrac{1}{2}\sin^2\tfrac{1}{2}\rho\,{\rm d}\rho\,\sin\theta\,{\rm d}\theta\,{\rm d}\phi, \tag{10.4}$$

where the group volume is $|\mathsf{SO(3)}|=2\pi^2$. This $N\times N$ matrix function $\mathbf{W}$ of meta-phase space $(x,p,\kappa)\in\mathcal{R}^3$ is in a sense the Fourier transform of the group, and we call it the *Wigner matrix* because it plays the same role for N-point signals on the classical sphere, as the well-known Wigner operator of quantum mechanics on the phase space plane. We shall not elaborate on the many properties of the

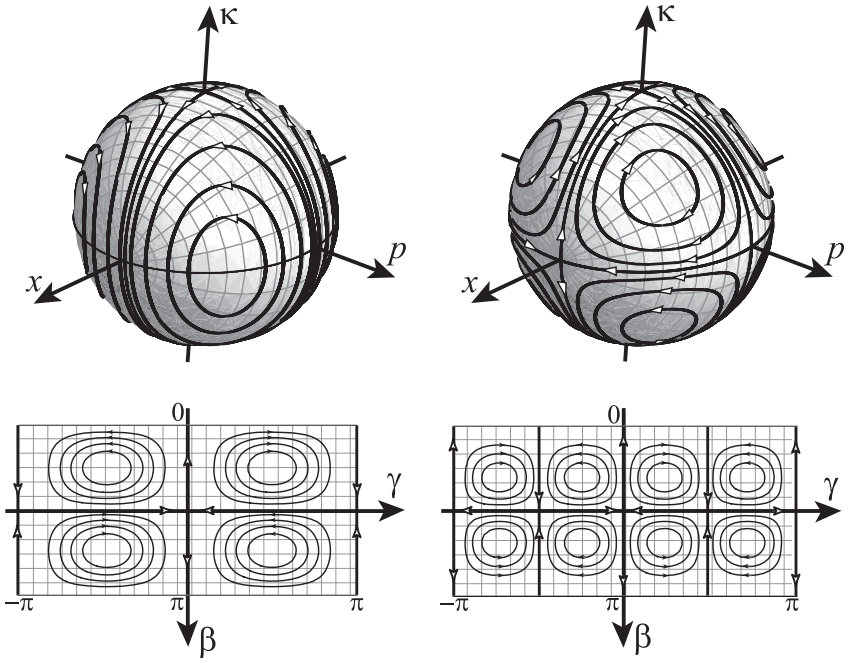

FIGURE 4. *Top row*: The Berezin classical space $(x, p, \kappa) \in \mathcal{R}^3$ and the lines of flow on the sphere produced by typical aberrations $-k < \mu < k$. *Bottom row*: Maps of the sphere (θ, ϕ) onto the bounded patch of the plane $0 \le \theta \le \pi$, $-\pi < \phi \le \pi$; the bottom pole falls on the center of the rectangle, the left and right edges are understood as contiguous, and the top and bottom edges represent a single point each of the position x-axis. *Left column*: Aberrations $A^{k,\mu;0}(x, p)$ in (8.5) belonging to the first pyramid (8.7), divide the sphere into quadrants of closed, nested lines. *Right column*: Aberrations $A^{k,\mu;1}(x, p, \kappa)$ in (8.6) belonging to the second pyramid (8.8), divide the flow on the sphere into octants.

Wigner matrix (10.3), which include unitarity and self-adjointness, reality, 'almost'-positivity, idempotency and marginals. We find suggestive the following symbolic form

$$\mathbf{W}(x, p, \kappa) \quad \text{“=”} \quad \delta_{\mathrm{SO}(3)}(x - \mathbf{X})\ \delta_{\mathrm{SO}(3)}(p - \mathbf{P})\ \delta_{\mathrm{SO}(3)}(\kappa - \mathbf{K}), \tag{10.5}$$

as if the matrices were classical quantities too, with a 'group-Dirac-δ' that should be properly defined. If true, we expect that the square radius of the sphere $x^2+p^2+\kappa^2 = r^2$ correspond with the value $j(j+1)$ of the Casimir operator (2.15), and that the significantly nonzero part of $\mathbf{W}(x, p, \kappa)$ be in the range $j < r < j+1$ —which in fact occurs [**28**].

For a given signal N-vector $\mathbf{f} = \{f_m\}_{m=-j}^{j}$, its $\mathsf{SO(3)}$ Wigner *function* is the expectation value of the Wigner matrix $\mathbf{W}(x, p, \kappa)$ in the state $\mathbf{f}$; it is the bilinear

form

$$W_{\mathrm{SO}(3)}(\mathbf{f}\,|\,x,p,\kappa\,) := \mathbf{f}^{\dagger}\,\mathbf{W}(x,p,\kappa)\,\mathbf{f} = \sum_{m,m'=-j}^{j} f_m^{*}\,W^{(j)}_{m,m'}(x,p,\kappa)\,f_{m'}, \tag{10.6}$$

The Wigner matrix elements $W^{(j)}_{m,m'}(x,p,\kappa)$ contain the integral (10.3) over the group manifold (ρ,θ,ϕ); this can be performed covariantly over the sphere (θ,ϕ) using the Wigner little-d rotation matrices [**28**], and then we slice the function at $\rho = r$ so that the matrix elements are reduced to the form

$$W^{(j)}_{m,m'}(r,\theta,\phi) = e^{-\mathrm{i}(m-m')\phi}\sum_{\bar m=-j}^{j} d^{j}_{m,\bar m}(\theta)\,\overline{W}^{(j)}_{\bar m}(r)\,d^{j}_{\bar m,m'}(-\theta), \tag{10.7}$$

where $\overline{W}^{(j)}_{\bar m}(r)$ are the elements of a diagonal matrix that is a function only of our chosen r. This can be expressed as an integral [**28**],

$$\begin{aligned}\overline{W}^{(j)}_{\bar m}(r) \quad &= \quad (-1)^{2j+1}\frac{\pi}{2}\sum_{m=-j}^{j}\int_0^{\pi}\sin\theta\,\mathrm{d}\theta \\ &\qquad \times |d^{j}_{\bar m,m}(\theta)|^2\frac{\sin(2\pi r\cos\theta)}{(r\cos\theta-m)[(r\cos\theta-m)^2-1]}.\end{aligned} \tag{10.8}$$

These N constants $\overline{W}^{(j)}_{\bar m}(r)$ we called the *Wigner constants* for each dimension $N = 2j+1$. The integral can be solved analytically, but we have found it more convenient to calculate their values by computer and store them, so that the rest of the algorithm consists of implementing (10.6)–(10.7) for any given signal $\mathbf{f}$ and (θ,ϕ) over the sphere by the symbolic and graphics program. This is practical on a PC up to about $N \approx 65$, or $j \approx 32$.

In Figures 5 and 6 we show the Wigner function for a discrete symmetric rectangle signal ($\mathrm{Rect}_L(m) = 1$ for $-j < -L \le m \le L < j$ and zero elsewhere), to be compared with its transformations under the first and second pyramid of aberrations in (8.7)–(8.8). In the first pyramid, we can see that the features around the center of the plot (the bottom pole of the sphere) transform consistently with those in Fig. 3. Those in the second pyramid contain a factor of $\kappa \leftrightarrow \mathcal{K}$, which seems to introduce a rotation around the center. These figures have appeared also in Ref. [**16**], although in a different format .

11. Conclusions

The exploration of discrete Hamiltonian systems is an ongoing process where our primary aim has been to evince the phase-space properties of the three quadratic systems: the harmonic and repulsive oscillators, and the free system —in one dimension. The finite oscillator that we reviewed here is under the ægis of SO(3), and can be said to be reasonably well understood [**16**]. Free systems under ISO(2) were touched upon some time ago [**6**] regarding wavefunctions, evolution, and Wigner function on a cylindrical phase space. The radius of this cylinder is proportional to the wavenumber of the field, so a field which is a continuous superposition of all wavelengths (colors) can be represented on a three-dimensional

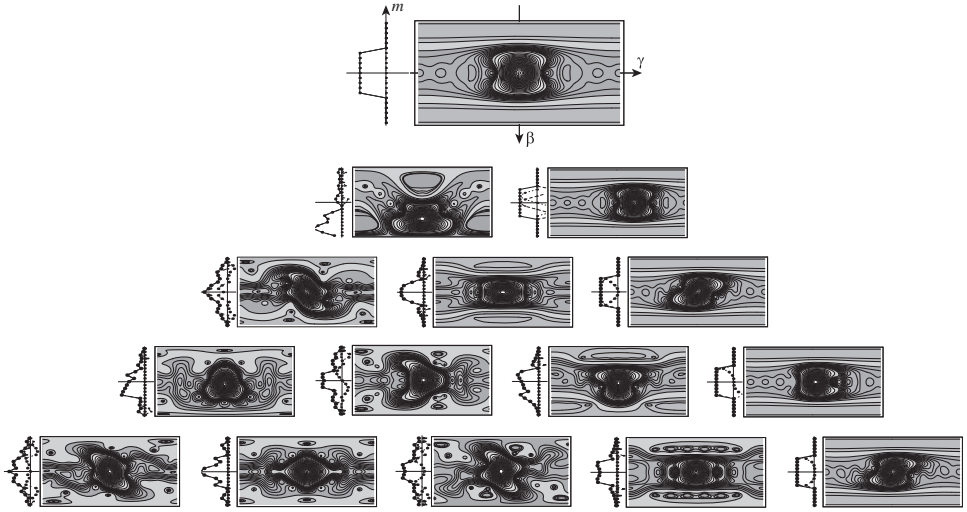

FIGURE 5. The first pyramid of aberrations up to order $A = 4$. *Top row*: Rectangle function $\mathrm{Rect}_4(m)$ shown left as an $N = 21$-point signal and right by its Wigner function on the (β, γ) manifold of the sphere, which projected onto the patch of the plane as in the left side of the previous Fig. 4, where the flux lines separate the sphere into quadrants. The marginal of the Wigner function, integrated horizontally, will yield the (sinc-interpolated) absolute square of the signal points [**16**, Eq. (A.6)]. *Rows 2,3,4,5*: Aberrations of order $A = 1$ (corresponding to x- and p-translations, $A^{1/2,1/2;0}$ and $A^{1/2,-1/2;0}$); order $A = 2$ (counterparts to the linear transformations in Fig. 3, $A^{1,1;0}$, $A^{1,0;0}$, and $A^{1,-1;0}$); order $A = 3$ ($A^{3/2,\mu;0}$, for $\mu = \frac{3}{2}, \frac{1}{2}, -\frac{1}{2}, -\frac{3}{2}$), and order $A = 4$ ($A^{2,\mu;0}$, $2 \geq \mu \geq -2$). The contour lines are drawn to resolve the near-zero values of the Wigner function: 0.0, ± 0.0001, ± 0.001, ± 0.01, 0.02, 0.03, ..., 0.15, 0.2, 0.3, ..., 3.0, 3.1.

space of nested cylinders. The discrete repulsive oscillator model for infinite discrete signals has been treated in Ref. [**10**]. Finally, for the paraxial regime of optics, a Wigner function on an $\mathcal{R}^3$ space with a third axis of 'color' was introduced in Ref. [**30**] on the Heisenberg-Weyl group.

Basing our construction on raising and lowering generators in Lie algebras implies that the position operator will always have equally-spaced eigenvalues. If instead we base our model on q-algebras we can obviate this limitation. Indeed, with $\mathsf{SU}_q(2)$, we obtained a model where the sensor points crowd towards the center, allowing for a higher resolution of the signals in this region [**32, 33**]. In the direction of applications we may compare the discrete with the continuous rendering of signals. For finite systems the comparison is made between the orthonormal basis of Kravchuk functions (5.4) and —most common— the sampled Hermite-Gauss functions used in wave optics [**31**]. Although with orthonormal bases we can restore the N-point signal exactly, it turns out that the non-orthogonal bases

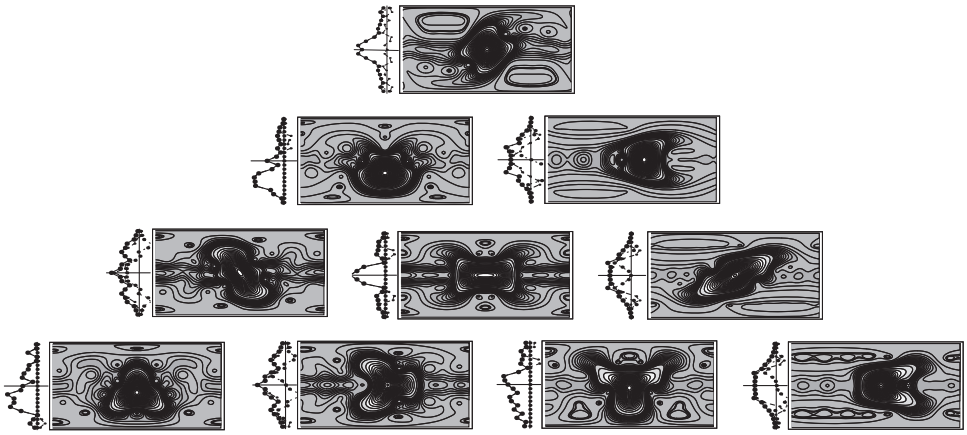

FIGURE 6. The second pyramid of aberrations up to order $A = 4$. *Top row*: Aberration of order 1; the same rectangle function $\mathrm{Rect}_4(m)$ of the previous figure under a 45° rotation (square root of the Fourier-Kravchuk transform) generated by $K = A^{0,0,1}$, and its Wigner function. *Second row*: Effect of aberrations of order 2, $A^{1/2,1/2;1}$ and $A^{1/2,-1/2;1}$ (which are $\mathcal{K}$-repeaters of the translations in the previous figure, $A^{1/2,1/2;0}$ and $A^{1/2,-1/2;0}$). *Following rows*: Aberrations of order 3, $A^{1,1;1}$, $A^{1,0;1}$, and $A^{1,-1;1}$ ($\mathcal{K}$-repeaters of the three $\mathsf{SO}(3)$-linear transformations $A^{1,\mu;0}$ of the previous figure), and order 4, $A^{3/2,\mu;0}$, for $\frac{3}{2} \geq \mu \geq -\frac{3}{2}$). Signals and their Wigner functions are laid out as in the previous figure, and correspond to maps whose flow divides the sphere into octants, as in the right of Fig. 4.

obtained by sampling gain the upper hand when we are interested in performing an approximate mode analysis of the signal with fewer than N terms terms.

We have broached the subject of separation of discrete variables: two-dimensional discrete systems can be built with sensor points arranged following either cartesian or polar coordinates [**34, 35**], corresponding with the group-subgroup chains $\mathsf{SO}(4) \supset \mathsf{SO}(2) \otimes \mathsf{SO}(2)$ or $\mathsf{SO}(4) \supset \mathsf{SO}(3) \supset \mathsf{SO}(2)$, respectively. Thus one finds counterparts for the Hermite-Gauss and Laguerre-Gauss beams [**36**], which in turn serve to rotate cartesian-pixellated images unitarily, and to map these onto polar-pixellated images —also unitarily [**37**]. Among the unsolved problems that may be addressed, we count the search for separating discrete coordinates of elliptic-hyperbolic pixellations of the plane. We hope that this succint exposition of $\mathsf{SO}(3)$ systems whets the reader's interest in group-theoretical models of discrete systems.

References

[1] K.B. Wolf, The Heisenberg–Weyl ring in quantum mechanics. In *Group Theory and its Applications, III*, Ed. by E.M. Loebl (Academic Press, Nueva York, 1975), pp. 189–247.

[2] E.P. Wigner, On the quantum correction for thermodynamic equilibrium, *Phys. Rev.* **40**, 749–759 (1932).

[3] M. Hillery, R.F. O'Connel, M.O. Scully, and E.P. Wigner, Distribution functions in physics: fundamentals, *Phys. Rep.* **259**, 121–167 (1984).

[4] K.B. Wolf, *Integral Transforms in Science and Engineering* (Plenum Publ. Corp., New York, 1979).
[5] L.C. Biedenharn and J.D. Louck, *Angular Momentum in Quantum Physics*, Encyclopedia of Mathematics and Its Applications, Ed. by G.-C. Rota (Addison-Wesley Publ. Co., Reading, Mass., 1981).
[6] L.M. Nieto, N.M. Atakishiyev, S.M. Chumakov, and K.B. Wolf, Wigner distribution function for Euclidean systems, *J. Phys. A* **31**, 3875–3895 (1998).
[7] M.A. Naĭmark, *Linear Representations of the Lorentz Group* (Pergamon Press, Oxford, 1964).
[8] N.M. Atakishiyev, Sh.M. Nagiyev, L.E. Vicent and K.B. Wolf, Covariant discretization of axis-symmetric linear optical systems. *J. Opt. Soc. Am. A* **17**, 2301–2314 (2000).
[9] V. Bargmann, Irreducible unitary representations of the Lorentz group, *Ann. Math.* **48**, 568–642 (1947).
[10] C. Muñoz, J. Rueda-Paz, and K.B. Wolf, Discrete repulsive oscillator wavefunctions, *J. Phys. A* **42**, 485210, 12*pp* (2009).
[11] N. M. Atakishiyev and K. B. Wolf, Fractional Fourier-Kravchuk transform, *J. Opt. Soc. Am. A* **14**, 1467–1477 (1997).
[12] N.M. Atakishiyev and S.K. Suslov, Difference analogs of the harmonic oscillator, *Theoret. and Math. Phys.* **85**, 1055–1062 (1991).
[13] N. M. Atakishiyev, G. S. Pogosyan, and K. B. Wolf, Finite models of the oscillator, *Phys. Part. Nuclei, Suppl. 3,* **36**, 521–555 (2005).
[14] N.M. Atakishiyev, G.S. Pogosyan and K.B. Wolf, Contraction of the finite one-dimensional oscillator, *Int. J. Mod. Phys. A* **18**, 317–327 (2003).
[15] V. Namias, The fractional order Fourier transform and its application to quantum mechanics, *J. Inst. Maths. Applics.* **25**, 241–265 (1980).
[16] K.B. Wolf, Linear transformations and aberrations in continuous and in finite systems, *J. Phys. A* **41**, art. 304026 (19 p.) (2008).
[17] K.B. Wolf, Discrete and finite fractional Fourier transforms. En: *Proceedings of the Workshop on Group Theory and Numerical Methods* (Université de Montréal, 26–31 May 2003), *CRM Proceedings and Lecture Series* Vol. **39**, 267–276 (2004).
[18] L. Barker, Ç. Candan, T. Hakioğlu, A. Kutay, and H.M. Ozaktas, The discrete harmonic oscillator, Harper's equation, and the discrete fractional Fourier transform, *J. Phys. A* **33**, 2209–2222 (2000).
[19] K. B. Wolf and G. Krötzsch, Geometry and dynamics in the fractional discrete Fourier transform, *J. Opt. Soc. Am. A* **24**, 651–658 (2007).
[20] K.B. Wolf, *Geometric Optics on Phase Space* (Springer-Verlag, Heidelberg, 2004).
[21] M. Moshinsky, J. Patera, R.T. Sharp, and P. Winternitz, Everything you ever wanted to know about $SU(3) \supset O(3)$, *Ann. Phys.* **95**, 139–150 (1975).
[22] A.J. Dragt, Elementary and advanced Lie algebraic methods with applications to accelerator design, electron microscopes, and light optics, *Nucl. Instr. Meth. Phys. Res. A* **258**, 339–354 (1987).
[23] J. Sánchez Mondragón and K.B. Wolf Eds. *Lie Methods in Optics*, Lecture Notes in Physics Vol. 250 (Springer Verlag, Heidelberg, 1986), Appendix B.
[24] I.M. Gel'fand and M.L. Tsetlin, Finite-dimensional representations of the group of unimodular matrices, *Dockl. akad. Nauk SSSR* **71**, 825-828 (1950); English translation in *I.M. Gel'fand, Collected Papers*, Vol. II (Springer-Verlag, Berlin, 1987) pp. 653–656.
[25] J.G. Nagel and M. Moshinsky, Operators that lower or raise the irreducible vector space of U_n, *J. Math. Phys.* **6**, 682–695 (1965).
[26] K.B. Wolf, The $U_{n,1}$ and IU_n representation matrix elements, *J. Math. Phys.* **13**, 1634–1638 (1972).
[27] H. M. Ozaktas, Z. Zalevsky, and M. Alper Kutay, *The Fractional Fourier Transform with Applications in Optics and Signal Processing* (Wiley, Chichester, 2001).
[28] N.M. Atakishiyev, S.M. Chumakov, and K.B. Wolf, Wigner distribution function for finite systems, *J. Math. Phys.* **39**, 6247–6261 (1998).
[29] S.T. Ali, N.M. Atakishiyev, S.M. Chumakov, and K.B. Wolf, The Wigner function for general Lie groups and the wavelet transform, *Ann. H. Poincaré* **1**, 685–714 (2000).
[30] K.B. Wolf, Wigner distribution function for paraxial polychromatic optics, *Opt. Commun.* **132**, 343–352 (1996).

[31] K.B. Wolf, Mode analysis and signal restoration with Kravchuk functions, *J. Opt. Soc. Am. A* **26**, 509–516 (2009).
[32] N.M. Atakishiyev, A.U. Klimyk and K.B. Wolf, Finite q-oscillator, *J. Phys. A* **37**, 5569–5587 (2004).
[33] N.M. Atakishiyev, A.U. Klimyk, and K.B. Wolf, Discrete quantum model of the harmonic oscillator, *J. Phys/ A* **41**, art. 085201, 14p. (2008).
[34] N.M. Atakishiyev, G.S. Pogosyan, L.E. Vicent and K.B. Wolf, Finite two-dimensional oscillator. I: The Cartesian model, *J. Phys. A* **34**, 9381–9398 (2001).
[35] N.M. Atakishiyev, G.S. Pogosyan, L.E. Vicent and K.B. Wolf, Finite two-dimensional oscillator. II: The radial model, *J. Phys. A* **34**, 9399–9415 (2001).
[36] K.B. Wolf and T. Alieva, Rotation and gyration of finite two-dimensional modes, *J. Opt. Soc. Am. A* **25**, 365–370 (2008).
[37] L.E. Vicent and K.B. Wolf, Unitary transformation between Cartesian- and polar-pixellated screens, *J. Opt. Soc. Am. A* **25**, 1875–1884 (2008).

Instituto de Ciencias Físicas, Universidad Nacional Autónoma de México, Av. Universidad s/n, Cuernavaca, Morelos 62210, México,
E-mail address: bwolf@fis.unam.mx